## LEAST-SQUARES NEURAL NETWORK (LSNN) METHOD FOR LINEAR ADVECTION-REACTION EQUATION: GENERAL DISCONTINUOUS INTERFACE \*

ZHIQIANG CAI†, JUNPYO CHOI†, AND MIN LIU‡

Abstract. We studied the least-squares ReLU neural network method (LSNN) for solving linear advection-reaction equation with discontinuous solution in [Cai, Zhiqiang, Jingshuang Chen, and Min Liu. "Least-squares ReLU neural network (LSNN) method for linear advection-reaction equation." Journal of Computational Physics 443 (2021): 110514]. The method is based on the least-squares formulation and employs a new class of approximating functions: multilayer perceptrons with the rectified linear unit (ReLU) activation function, i.e., ReLU deep neural networks (DNNs). In this paper, we first show that ReLU DNN with depth  $\lceil \log_2(d+1) \rceil + 1$  can approximate any d-dimensional step function on arbitrary discontinuous interfaces with any prescribed accuracy. By decomposing the solution into continuous and discontinuous parts, we prove theoretically that discretization error of the LSNN method using DNN with depth  $\lceil \log_2(d+1) \rceil + 1$  is mainly determined by the continuous part of the solution provided that the solution jump is constant. Numerical results for both two and three dimensional problems with various discontinuous interfaces show that the LSNN method with enough layers is accurate and does not exhibit the common Gibbs phenomena along interfaces.

Key words. Least-Squares Method, ReLU Neural Network, Linear Advection-Reaction Equation, Discontinuous Solution

MSC codes. 65N15, 65N99

1. Introduction. Let  $\Omega$  be a bounded domain in  $\mathbb{R}^d$   $(d \geq 2)$  with Lipschitz boundary  $\partial\Omega$ . Consider the linear advection-reaction equation

(1.1) 
$$\begin{cases} u_{\beta} + \gamma u = f, & \text{in } \Omega, \\ u = g, & \text{on } \Gamma_{-}, \end{cases}$$

where  $\beta(\mathbf{x}) = (\beta_1, \dots, \beta_d)^T \in C^0(\bar{\Omega})^d$  is a given advective velocity field,  $u_{\beta}$  denotes the directional derivative of u along  $\beta$ , and  $\Gamma_-$  is the inflow part of the boundary  $\Gamma = \partial \Omega$  given by

(1.2) 
$$\Gamma_{-} = \{ \mathbf{x} \in \Gamma : \boldsymbol{\beta}(\mathbf{x}) \cdot \boldsymbol{n}(\mathbf{x}) < 0 \}$$

with  $\mathbf{n}(\mathbf{x})$  the unit outward normal vector to  $\Gamma$  at  $\mathbf{x} \in \Gamma$ . Assume that  $\gamma \in C^0(\bar{\Omega})$ ,  $f \in L^2(\Omega)$ , and  $g \in L^2(\Gamma)$  are given scalar-valued functions.

When the inflow boundary data g is discontinuous, so is the solution of (1.1). The discontinuous interface may be determined by the characteristic curves emanating from where g is discontinuous. By using the location of the interface, one may design an accurate mesh-based numerical method. However, this type of methods is usually limited to linear problems and is difficult to be extended to nonlinear hyperbolic conservation laws.

In [7], we studied the least-squares ReLU neural network method (LSNN) for solving (1.1) with discontinuous solution. The method is based on the least-squares formulation analyzed in [11, 4] and employs a new class of approximating functions: multilayer perceptrons with the rectified linear unit (ReLU) activation function, i.e., ReLU deep neural networks (DNNs). One of the appealing features of the LSNN method is its ability of automatically approximating the discontinuous solution without using a priori knowledge of the location of the interface. Hence, the

<sup>\*</sup>Submitted to the editors DATE.

Funding: This work was supported in part by the National Science Foundation under grant DMS-2110571.

<sup>&</sup>lt;sup>†</sup>Department of Mathematics, Purdue University, 150 N. University Street, West Lafayette, IN 47907-2067 (caiz@purdue.edu, choi508@purdue.edu).

<sup>&</sup>lt;sup>‡</sup>School of Mechanical Engineering, Purdue University, 585 Purdue Mall, West Lafayette, IN 47907-2088(liu66@purdue.edu).

method is applicable to nonlinear problems (see [5, 6]). Compared to mesh-based numerical methods including various adaptive mesh refinement (AMR) algorithms that locate the discontinuous interface through local mesh refinement (see, e.g., [10, 16, 19]), the LSNN method, a meshfree and pointfree method, is much more effective in terms of the number of the degrees of freedom. Theoretically, it was shown in [7] that a two- or three-layer ReLU neural network in two dimensions is sufficient to well approximate the solution of (1.1) without oscillation, provided that the interface consists of a straight line or two-line segments and that the solution jump along the interface is constant.

The assumption on at most two-line segments in [7] is very restrictive even in two dimensions since, in general, the discontinuous solution of (1.1) has an interface that is a hyper-surface in d dimensions. The main purpose of this paper is to establish a priori error estimates (see Theorem 4.4) for the LSNN method in d dimensions for general discontinuous interface. To do so, we first derive a decomposition of the solution as the sum of the discontinuous and continuous parts (see (4.3)). Obviously, the continuous part of the solution may be approximated well by (even shallow) ReLU NNs with standard approximation property (see, e.g., [13, 20, 21, 23, 12]).

To deal with the main numerical difficulty of the problem, i.e., the discontinuous part of the solution, we notice that it may be represented by a step function along a hyper-surface interface if the solution jump is a constant. By an explicit construction, we show that this step function can be approximated by a continuous piecewise linear (CPWL) function with a sharp transition layer of  $\varepsilon$  width very accurately; more precisely, the error is bounded above by  $\mathcal{O}(J\sqrt{\varepsilon})$ , where J is the step size (see Lemma 4.3). Based on a recent result of the relationship between ReLU DNNs and CPWL functions in [1], using the main results in [25, 26], the explicitly constructed CPWL function belongs to the class of ReLU DNN  $\mathbb{R}^d \to \mathbb{R}$  with at most  $\lceil \log_2(d+1) \rceil + 1$  depth. Therefore, the discontinuous part of the solution can be approximated accurately by this class, provided that the solution jump is a constant.

The explicit construction indicates that DNNs with at most  $\lceil \log_2(d+1) \rceil + 1$  depth is sufficient to accurately approximate discontinuous solutions without oscillation. The necessary depth  $\lceil \log_2(d+1) \rceil + 1$  of a DNN is shown numerically through several test problems in both two and three dimensions. At the current stage, it is still very expensive to numerically solve the discrete least-squares minimization problem when using the ADAM optimization algorithm [17], even though the DoFs of the LSNN method is much less than mesh-based numerical methods.

Followed by recent success of DNNs in machine learning and artificial intelligence tasks such as computer vision and pattern recognition, there have been active interests in using DNNs for solving partial differential equations (PDEs) (see, e.g., [2, 3, 9, 14, 22, 24]). Due to the fact that the collection of DNN functions is not a space, NN methods for PDEs are often based on an equivalent optimization formulation of a PDE. This is why there are mainly two types of NN methods: the Ritz and least-squares (LS) methods. The former (see, e.g., [14]) requires the underlying problem having a natural minimization principle and hence is not applicable to (1.1). There are many LS formulations for a given PDE. Hence efficacy of the latter depends on a specific LS form. Most of them simply use the discrete LS formulation of the underlying PDE in its strong form and therefore are not applicable to (1.1).

The paper is organized as follows. In Section 2, we describe ReLU DNNs and CPWL functions, and introduce a known result about their relationship. Then we further investigate the structure of ReLU DNNs. Section 3 review the least-squares neural network method and formulate the method on the framework in Section 2. Then we prove the method is capable of locating any discontinuous interfaces of the problem in Section 4. Finally, Section 5 presents numerical results for both two and three dimensional test problems with various discontinuous interfaces.

2. ReLU DNN. First we begin with the definition of the rectified linear unit (ReLU) activation function. The ReLU activation function  $\sigma$  is defined by

$$\sigma(t) = \max\{0, t\} = \begin{cases} 0, & \text{if } t \le 0, \\ t, & \text{if } t > 0. \end{cases}$$

We say a function  $\mathcal{N}: \mathbb{R}^d \to \mathbb{R}^c$  with  $c, d \in \mathbb{N}$  is a ReLU deep neural network (DNN) if the function  $\mathcal{N}$  has a representation:

(2.1) 
$$\mathcal{N} = N^{(L)} \circ \cdots \circ N^{(2)} \circ N^{(1)} \text{ with } L > 1,$$

where the symbol  $\circ$  denotes the composition of functions, and for each  $l=1,\ldots,L,\,N^{(l)}:\mathbb{R}^{n_{l-1}}\to$  $\mathbb{R}^{n_l}$  with  $n_l, n_{l-1} \in \mathbb{N}$   $(n_0 = d, n_L = c)$  given by:

- 1. For l = L,  $N^{(L)}(\mathbf{x}) = \boldsymbol{\omega}^{(L)}\mathbf{x} \mathbf{b}^{(L)}$  for all  $\mathbf{x} \in \mathbb{R}^{n_{L-1}}$  for  $\boldsymbol{\omega}^{(L)} \in \mathbb{R}^{n_L \times n_{L-1}}$ ,  $\mathbf{b}^{(L)} \in \mathbb{R}^{n_L}$ . 2. For each  $l = 1, \ldots, L-1$ ,  $N^{(l)}(\mathbf{x}) = \sigma(\boldsymbol{\omega}^{(l)}\mathbf{x} \mathbf{b}^{(l)})$  for all  $\mathbf{x} \in \mathbb{R}^{n_{l-1}}$  for  $\boldsymbol{\omega}^{(l)} \in \mathbb{R}^{n_l \times n_{l-1}}$ ,  $\mathbf{b}^{(l)} \in \mathbb{R}^{n_l}$ , where  $\sigma$  is applied to each component.

We now establish terminology as follows. Let a ReLU DNN  $\mathcal{N}$  have a representation  $N^{(L)} \circ \cdots \circ$  $N^{(2)} \circ N^{(1)}$  with L > 1 as in (2.1). Then we say:

- 1. The representation has depth L.
- 2. The representation is said to have L layers and L-1 hidden layers.
- 3. For each l = 1, ..., L, the entries of  $\boldsymbol{\omega}^{(l)}$  and  $\mathbf{b}^{(l)}$  are called weights and biases, respectively.
- 4. For each l = 1, ..., L, the natural number  $n_l$  is called the width or the number of neurons of the  $l^{\text{th}}$  layer.

A motivation for this terminology is illustrated in Figure 1.

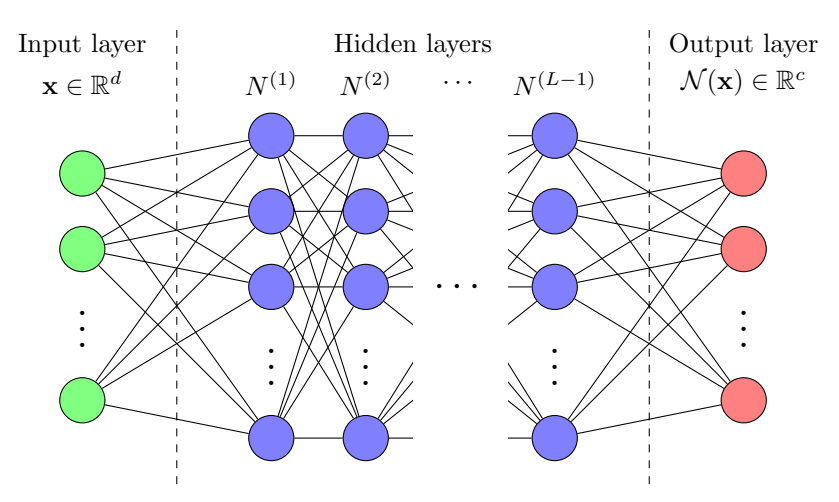


Fig. 1. ReLU Deep Neural Network

For a given positive integer n, denote the set of ReLU DNNs from  $\mathbb{R}^d$  to  $\mathbb{R}$  that have representations with depth L and the total number of neurons in the hidden layers n by

$$\mathcal{M}(d,1,L,n) = \left\{ \mathcal{N} : \mathbb{R}^d \to \mathbb{R} : \mathcal{N} = N^{(L)} \circ \cdots \circ N^{(2)} \circ N^{(1)} \text{ defined in } (2.1) : n = \sum_{l=1}^{L-1} n_l \right\}.$$

Denote the set of all ReLU DNNs from  $\mathbb{R}^d$  to  $\mathbb{R}$  with L-layer representations by  $\mathcal{M}(d,1,L)$ . Then

(2.2) 
$$\mathcal{M}(d,1,L) = \bigcup_{n \in \mathbb{N}} \mathcal{M}(d,1,L,n).$$

We now introduce another function class, which is the set of continuous piecewise linear functions, and explore a theorem about the relationship between the two function classes. We say a function  $f: \mathbb{R}^d \to \mathbb{R}$  with  $d \in \mathbb{N}$  is continuous piecewise linear (CPWL) if there exists a finite set of polyhedra with nonempty interior such that:

- 1. The interiors of any two polyhedra in the set are disjoint.
- 2. The union of the set is  $\mathbb{R}^d$ .
- 3. f is affine linear over each polyhedron in the set, i.e., in each polyhedron in the set,  $f(\mathbf{x}) = \mathbf{a}^T \mathbf{x} + b$  for  $\mathbf{a} \in \mathbb{R}^d$ ,  $b \in \mathbb{R}$ .

Here by a polyhedron, we mean a subset of  $\mathbb{R}^d$  surrounded by a finite number of hyper-planes, i.e., the solution set of a system of linear inequalities

(2.3) 
$$\{\mathbf{x} \in \mathbb{R}^d : \mathbf{A}\mathbf{x} \le \mathbf{b}\} \text{ for } \mathbf{A} \in \mathbb{R}^{m \times d}, \mathbf{b} \in \mathbb{R}^m \text{ with } m \in \mathbb{N},$$

where the inequality is applied to each component. Thus the interior of the polyhedron in (2.3) is

$$\{\mathbf{x} \in \mathbb{R}^d : \mathbf{A}\mathbf{x} < \mathbf{b}\}.$$

PROPOSITION 2.1. The set of CPWL functions  $f: \mathbb{R}^d \to \mathbb{R}$  is equal to  $\mathcal{M}(d, 1, \lceil \log_2(d+1) \rceil + 1)$ , i.e., the set of ReLU DNNs from  $\mathbb{R}^d$  to  $\mathbb{R}$  that have representations with depth  $\lceil \log_2(d+1) \rceil + 1$ .

*Proof.*  $\mathcal{M}(d,1,\lceil \log_2(d+1)\rceil+1)$  is clearly a subset of the set of CPWL functions. Conversely, it is proved in [1] that every CPWL function is a ReLU DNN from  $\mathbb{R}^d$  to  $\mathbb{R}$  that has a representation with depth at most  $\lceil \log_2(d+1) \rceil + 1$ . Now, the result follows from the fact that  $\mathcal{M}(d,1,L) \subset \mathcal{M}(d,1,\lceil \log_2(d+1)\rceil+1)$  for any  $L \leq \lceil \log_2(d+1)\rceil+1$ .

Proposition 2.1 enables us to employ ReLU DNNs with a few layer representations to the problems where CPWL functions are used, and to only control the number of neurons. Except the case d=1 (see, e.g., [1]), there are currently no known results to give tight bounds on the number of neurons in the hidden layers. Therefore we suggest the following approach. The following proposition is a trivial fact.

Proposition 2.2.  $\mathcal{M}(d, 1, L, n) \subset \mathcal{M}(d, 1, L, n + 1)$ .

Now Proposition 2.1 (2.2), and Proposition 2.2 suggest how we control the number of neurons in the hidden layers, i.e., when approximating a function  $\mathbb{R}^d \to \mathbb{R}$  by a CPWL function  $\mathbb{R}^d \to \mathbb{R}$ , we start with a class  $\mathcal{M}(d, 1, \lceil \log_2(d+1) \rceil + 1, n)$  with a small n, and then increase n to have a better approximation.

3. LSNN Method. Define the least-squares (LS) functional as

(3.1) 
$$\mathcal{L}(v; \mathbf{f}) = \|v_{\beta} + \gamma v - f\|_{0,\Omega}^2 + \|v - g\|_{-\beta}^2,$$

where  $\mathbf{f} = (f, g)$  and  $\|\cdot\|_{-\beta}$  denotes the weighted  $L^2(\Gamma_-)$  norm over the inflow boundary given by

$$\|v\|_{-\boldsymbol{\beta}} = \langle v, v \rangle_{-\boldsymbol{\beta}}^{1/2} = \left( \int_{\Gamma_{-}} |\boldsymbol{\beta} \cdot \boldsymbol{n}| \, v^2 \, ds \right)^{1/2}.$$

Let  $V_{\beta} = \{v \in L^2(\Omega) : v_{\beta} \in L^2(\Omega)\}$  that is equipped with the norm as

$$|||v|||_{\boldsymbol{\beta}} = (||v||_{0,\Omega}^2 + ||v_{\boldsymbol{\beta}}||_{0,\Omega}^2)^{1/2}.$$

The least-squares formulation of problem (1.1) is to seek  $u \in V_{\beta}$  such that

(3.2) 
$$\mathcal{L}(u; \mathbf{f}) = \min_{v \in V_{\mathcal{B}}} \mathcal{L}(v; \mathbf{f}).$$

PROPOSITION 3.1 (see [4, 11]). Assume that either  $\gamma = 0$  or there exists a positive constant  $\gamma_0$  such that

(3.3) 
$$\gamma(\mathbf{x}) - \frac{1}{2} \nabla \cdot \boldsymbol{\beta}(\mathbf{x}) \ge \gamma_0 > 0 \quad \text{for almost all } \mathbf{x} \in \Omega.$$

Then the homogeneous LS functional  $\mathcal{L}(v; \mathbf{0})$  is equivalent to the norm  $|||v|||_{\beta}^2$ , i.e., there exist positive constants  $\alpha$  and M such that

(3.4) 
$$\alpha \|\|v\|_{\beta}^{2} \leq \mathcal{L}(v; \mathbf{0}) \leq M \|\|v\|_{\beta}^{2} \quad \text{for all } v \in V_{\beta}.$$

Proposition 3.2 (see [4, 11]). Problem (3.2) has a unique solution  $u \in V_{\beta}$  satisfying the following a priori estimate

$$|||u|||_{\beta} \le C \left(||f||_{0,\Omega} + ||g||_{-\beta}\right).$$

Note that  $\mathcal{M}(d, 1, L, n)$  is a subset of  $V_{\beta}$ . The least-squares approximation is to find  $u_N \in \mathcal{M}(d, 1, L, n)$  such that

(3.6) 
$$\mathcal{L}(u_N; \mathbf{f}) = \min_{v \in \mathcal{M}(d, 1, L, n)} \mathcal{L}(v; \mathbf{f}).$$

Lemma 3.3 (see [7]). Let u and  $u_{\scriptscriptstyle N}$  be the solutions of problems (3.2) and (3.6), respectively. Then we have

(3.7) 
$$|||u - u_{N}|||_{\beta} \le \left(\frac{M}{\alpha}\right)^{1/2} \inf_{v \in \mathcal{M}(d, 1, L, n)} |||u - v|||_{\beta},$$

where  $\alpha$  and M are constants in (3.4).

We use numerical integration (the midpoint rule) to implement the scheme in (3.6) (see [7]). Denote the discrete LS functional by  $\mathcal{L}_{\tau}(v; \mathbf{f})$  for  $v \in V_{\beta}$ . Then the discrete least-squares approximation of problem (1.1) is to find  $u_{\tau}^{N} \in \mathcal{M}(d, 1, L, n)$  such that

(3.8) 
$$\mathcal{L}_{\tau}(u_{\tau}^{N}; \mathbf{f}) = \min_{v \in \mathcal{M}(d.1, L, n)} \mathcal{L}_{\tau}(v; \mathbf{f}).$$

4. Error Estimate. In this section, we provide error estimates of the ReLU DNN approximations to the solution of the linear advection-reaction equation with an arbitrary discontinuous interface. To this end, we notice first that the solution of the problem is discontinuous if the inflow boundary data g is discontinuous.

LEMMA 4.1. For d=2, assume that the inflow boundary data g is discontinuous at  $\mathbf{x}_0 \in \Gamma_-$  with values  $g^+(\mathbf{x}_0)$  and  $g^-(\mathbf{x}_0)$  from different sides. Let I be the streamline of the vector field  $\boldsymbol{\beta}$  emanating from  $\mathbf{x}_0$ , and let  $\mathbf{x}(s)$  be a parameterization of I, i.e.,

(4.1) 
$$\frac{d\mathbf{x}(s)}{ds} = \boldsymbol{\beta}(\mathbf{x}(s)), \quad \mathbf{x}(0) = \mathbf{x}_0.$$

Then the solution u of (1.1) is discontinuous on I with jump described as

$$|u^{+}(\mathbf{x}(s)) - u^{-}(\mathbf{x}(s))| = \exp\left(-\int_{0}^{s} \gamma(\mathbf{x}(t)) dt\right) \left| \int_{0}^{s} \exp\left(\int_{0}^{t} \gamma(\mathbf{x}(r)) dr\right) (f^{+}(\mathbf{x}(t)) - f^{-}(\mathbf{x}(t))) dt + g^{+}(\mathbf{x}_{0}) - g^{-}(\mathbf{x}_{0})\right|,$$

where  $u^+(\mathbf{x}(s))$  and  $u^-(\mathbf{x}(s))$  are the solutions, and  $f^+(\mathbf{x}(t))$  and  $f^-(\mathbf{x}(t))$  are the values of f of (1.1) along I from different sides, respectively.

*Proof.* Along the interface I, by the definition of the directional derivative, we have

$$u_{\beta}(\mathbf{x}(s)) = \frac{d}{ds}u(\mathbf{x}(s)).$$

Thus the solutions  $u^{\pm}(\mathbf{x}(s))$  along the interface I satisfies the linear ordinary differential equations

(4.2) 
$$\begin{cases} \frac{d}{ds}u^{\pm}(\mathbf{x}(s)) + \gamma(\mathbf{x}(s))u^{\pm}(\mathbf{x}(s)) &= f^{\pm}(\mathbf{x}(s)), & \text{for } s > 0, \\ u^{\pm}(\mathbf{x}(0)) &= u^{\pm}(\mathbf{x}_0) = g^{\pm}(\mathbf{x}_0), \end{cases}$$

whose solutions are given by

$$u^{\pm}(\mathbf{x}(s)) = \exp\left(-\int_0^s \gamma(\mathbf{x}(t)) dt\right) \left[\int_0^s \exp\left(\int_0^t \gamma(\mathbf{x}(r)) dr\right) f^{\pm}(\mathbf{x}(t)) dt + g^{\pm}(\mathbf{x}_0)\right].$$

Hence, u is discontinuous on I with jump

$$|u^{+}(\mathbf{x}(s)) - u^{-}(\mathbf{x}(s))| = \exp\left(-\int_{0}^{s} \gamma(\mathbf{x}(t)) dt\right) \left| \int_{0}^{s} \exp\left(\int_{0}^{t} \gamma(\mathbf{x}(r)) dr\right) (f^{+}(\mathbf{x}(t)) - f^{-}(\mathbf{x}(t))) dt + g^{+}(\mathbf{x}_{0}) - g^{-}(\mathbf{x}_{0})\right|.$$

This completes the proof of the lemma.

Remark 4.2. For d=3, assume that the inflow boundary data g is discontinuous along a curve  $C(t) \subset \Gamma_-$ . Note the collection of the stream lines  $\mathbf{x}(s)$  of the vector field  $\boldsymbol{\beta}$  starting at all  $\mathbf{x}_0 = C(t)$  forms a surface I(s,t). Then the solution u of (1.1) is discontinuous on the surface I(s,t) with jump as in Lemma 4.1 for every  $\mathbf{x}_0 = C(t)$ .

Let the solution u of (1.1) be discontinuous across an interface I due to a discontinuity of the inflow boundary condition g. For example, in  $\mathbb{R}^2$ , an interface can be the streamline emanating from  $\mathbf{x}_0$  at which g is discontinuous. Let I divide the domain  $\Omega$  into two non-empty subdomains  $\Omega_1$  and  $\Omega_2$ :

$$\Omega = \Omega_1 \cup \Omega_2$$
 and  $I = \partial \Omega_1 \cap \partial \Omega_2$ ,

so that u is piece-wise smooth with respect to the partition  $\{\Omega_1, \Omega_2\}$ .

Assume that the jump of the solution is a constant. Hence, u can be decomposed into

$$u(\mathbf{x}) = \hat{u}(\mathbf{x}) + \chi(\mathbf{x}),$$

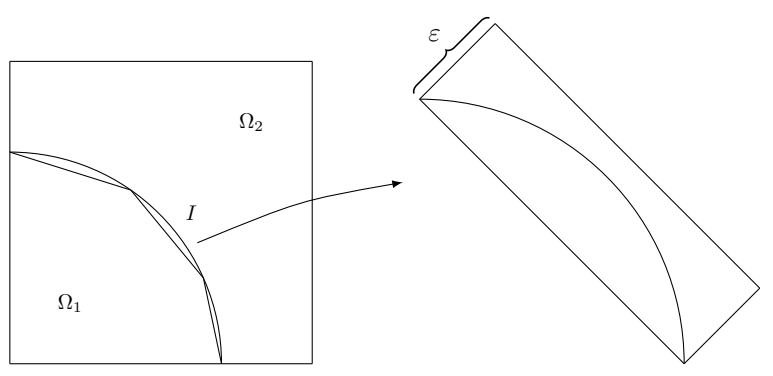
where  $\hat{u}$  is continuous and piece-wise smooth in  $\Omega$ , and  $\chi(\mathbf{x})$  is a piece-wise constant function defined by

$$\chi(\mathbf{x}) = \begin{cases} \alpha_1, & \mathbf{x} \in \Omega_1, \\ \alpha_2, & \mathbf{x} \in \Omega_2 \end{cases}$$

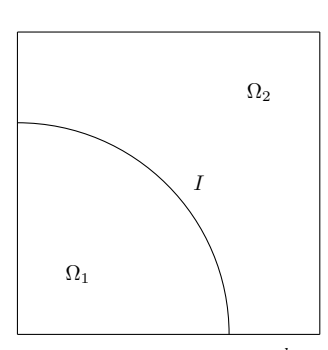
with  $\alpha_1 = g^-(\mathbf{x}_0)$  and  $\alpha_2 = g^+(\mathbf{x}_0)$  (see Figure 2(b)). By a rotation of the coordinates  $\mathbf{x}$ , we represent the interface I by  $s = R(\mathbf{y})$ . Next for any  $\varepsilon > 0$ , we approximate R by a CPWL function  $s = c(\mathbf{y})$  with linear functions  $c_i(\mathbf{y})$ , i = 1, ..., k such that the vertical distance from  $c_i$  to the corresponding portion of I is less than  $\varepsilon$  (see Figure 2(a)). Each linear function  $c_i(\mathbf{y})$  of R is a hyperplane  $\boldsymbol{\xi}_i \cdot \mathbf{x} = b_i$ . By normalizing  $\boldsymbol{\xi}_i$ , we can assume  $|\boldsymbol{\xi}_i| = 1$ . We now divide  $\Omega$  by hyperplanes passing through the intersections of  $\boldsymbol{\xi}_i \cdot \mathbf{x} = b_i$ . Let  $\Upsilon_i$  be the subdomains determined by this process (see Figure 2(c)).

LEMMA 4.3. Without loss of generality, let  $p(\mathbf{x})$  be a CPWL function given by (see Figure 2(d))

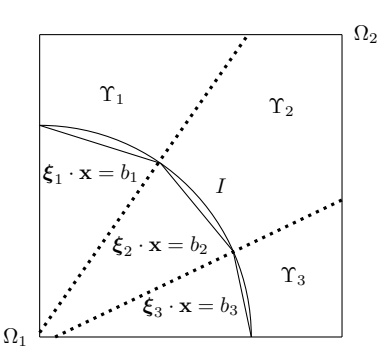
$$p_i(\mathbf{x}) = \alpha_1 + \frac{\alpha_2 - \alpha_1}{\varepsilon} \Big( \sigma(\boldsymbol{\xi}_i \cdot \mathbf{x} - b_i) - \sigma(\boldsymbol{\xi}_i \cdot \mathbf{x} - b_i - \varepsilon) \Big), \ \mathbf{x} \in \Upsilon_i.$$



(a) Approximation along the interface  ${\cal I}$  by a CPWL function



(b) Interface I in  $\Omega \subset \mathbb{R}^d$ 



(c) Partition of  $\Omega$  through the intersections of  $\pmb{\xi}_i \cdot \mathbf{x} = b_i$ 

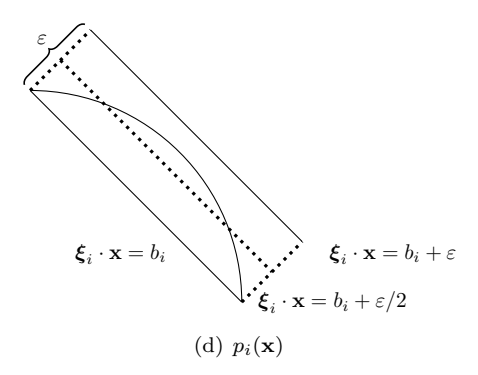


Fig. 2. Lemma 4.3 illustruations

Then we have

(4.4) 
$$\|\chi - p\|_{\beta} \le \sqrt{2|I|} \left| \alpha_1 - \alpha_2 \right| \sqrt{\varepsilon},$$

where |I| is the d-1 dimensional measure of the interface I.

*Proof.* For each i, denote by  $|\mathcal{P}_i|$  the d-1 dimensional measure of the hyperplane  $\boldsymbol{\xi}_i \cdot \mathbf{x} = b_i$  in  $\Upsilon_i$ . It is easy to check that

$$\|\chi - p_i\|_{0,\Upsilon_i}^2 \le (\alpha_1 - \alpha_2)^2 |\mathcal{P}_i| \varepsilon,$$

which implies

$$(4.5) \|\chi - p\|_{0,\Omega}^2 = \sum_{i=1}^k \|\chi - p_i\|_{0,\Upsilon_i}^2 \le \sum_{i=1}^k |\mathcal{P}_i| (\alpha_1 - \alpha_2)^2 \varepsilon \le |I| (\alpha_1 - \alpha_2)^2 \varepsilon.$$

We now prove

$$\|\chi_{\boldsymbol{\beta}} - p_{\boldsymbol{\beta}}\|_{0,\Omega}^2 \le |I| (\alpha_1 - \alpha_2)^2 \varepsilon.$$

To do so, for each i, let

$$\Upsilon_i^1 = \{ \mathbf{x} \in \Upsilon_i : 0 < \boldsymbol{\xi} \cdot \mathbf{x} - b_i < \varepsilon \} \text{ and } \Upsilon_i^2 = \Upsilon_i \setminus \Upsilon_i^1.$$

Clearly,  $\chi_{\boldsymbol{\beta}} \equiv 0$  in  $\Omega$ , and  $p_i$  is piecewise constant in  $\Upsilon_i^2$ . For each  $\Upsilon_i$ , we can construct vector-field  $\boldsymbol{\beta}_i(\mathbf{x})$  in  $\Upsilon_i$  such that for each  $\mathbf{x} \in \Upsilon_i^1$ ,  $\boldsymbol{\beta}_i(\mathbf{x})$  is parallel to the hyperplane  $\boldsymbol{\xi}_i \cdot \mathbf{x} = b_i$  in  $\Upsilon_i$  and that  $\boldsymbol{\beta}(\mathbf{x}) - \boldsymbol{\beta}_i(\mathbf{x})$  is parallel to  $\boldsymbol{\xi}_i$  in  $\Upsilon_i^1$ . Hence,  $(p_i)_{\boldsymbol{\beta}_i} \equiv 0$  in  $\Upsilon_i$ . Then

$$\begin{aligned} \|(p_i)_{\boldsymbol{\beta}}\|_{0,\Upsilon_i}^2 &= \|(p_i)_{\boldsymbol{\beta}} - (p_i)_{\boldsymbol{\beta}_i}\|_{0,\Upsilon_i}^2 = \|(p_i)_{\boldsymbol{\beta} - \boldsymbol{\beta}_i}\|_{0,\Upsilon_i}^2 = \|(p_i)_{\boldsymbol{\beta} - \boldsymbol{\beta}_i}\|_{0,\Upsilon_i}^2 \\ &\leq \int_{\Upsilon_i^1} \left(\frac{\alpha_2 - \alpha_1}{\varepsilon} \boldsymbol{\xi}_i \cdot \varepsilon \boldsymbol{\xi}_i\right)^2 d\mathbf{x} \leq (\alpha_1 - \alpha_2)^2 |\mathcal{P}_i| \,\varepsilon, \end{aligned}$$

where for the second inequality, we used the fact that in  $\Upsilon_i^1$ , the gradient of  $p_i$  is  $\frac{\alpha_2 - \alpha_1}{\varepsilon} \xi_i$  and the magnitude of  $\beta(\mathbf{x}) - \beta_i(\mathbf{x})$  is less than or equal to  $\varepsilon \xi_i$ . Thus

Now (4.4) follows from (4.5) and (4.6).

Theorem 4.4. Let u and  $u_N$  be the solutions of problems (3.2) and (3.6), respectively. Then we have

where  $\hat{u} \in C(\Omega)$  and p are given in (4.3) and Lemma 4.3, respectively. Moreover, if the depth of DNNs in (3.6) is at least  $\lceil \log_2(d+1) \rceil + 1$ , then for a sufficiently large integer n, there exists an integer  $\hat{n} \leq n$  such that

where  $\mathcal{M}(d, n - \hat{n}) = \mathcal{M}(d, 1, \lceil \log_2(d+1) \rceil + 1, n - \hat{n}).$ 

*Proof.* For any  $v \in \mathcal{M}(d, 1, L, n)$ , it follows from (4.3), the triangle inequality, and Lemma 4.3 that

$$\begin{split} \| u - v \|_{\beta} &= \| | \chi - p + \hat{u} + p - v \|_{\beta} \le \| | \chi - p \|_{\beta} + \| | \hat{u} + p - v \|_{\beta} \\ &\le \sqrt{2|I|} |\alpha_1 - \alpha_2| \sqrt{\varepsilon} + \| | \hat{u} + p - v \|_{\beta}. \end{split}$$

Taking the infimum over all  $v \in \mathcal{M}(d, 1, L, n)$ , (4.7) is then a direct consequence of Lemma 3.3.

For a sufficiently large integer n, by Proposition 2.1, there exists an integer  $\hat{n} \leq n$  such that

$$p \in \mathcal{M}(d, \hat{n}) = \mathcal{M}(d, 1, \lceil \log_2(d+1) \rceil + 1, \hat{n}).$$

Obviously we have  $v + p \in \mathcal{M}(d, n)$  for any  $v \in \mathcal{M}(d, n - \hat{n})$ . Now, it follows from the coercivity and continuity of the homogeneous functional  $\mathcal{L}(v; \mathbf{0})$  in (3.4), problems (1.1), (3.6), (4.3), and the triangle inequality that

$$\alpha \|\|u - u_N\|_{\boldsymbol{\beta}}^2 \le \mathcal{L}(u - u_N; \mathbf{0}) = \mathcal{L}(u_N; \mathbf{f}) \le \mathcal{L}(v + p; \mathbf{f}) = \mathcal{L}(u - v - p; \mathbf{0})$$

$$= \mathcal{L}((\hat{u} - v) + (\chi - p); \mathbf{0}) \le M \|(\hat{u} - v) + (\chi - p)\|_{\boldsymbol{\beta}}^2$$

$$\le 2M \left( \|\|(\hat{u} - v)\|_{\boldsymbol{\beta}}^2 + \|(\chi - p)\|_{\boldsymbol{\beta}}^2 \right),$$

which, together with Lemma 4.3, implies the validity of (4.8). This completes the proof of the theorem.

Remark 4.5. When the continuous part of the solution  $\hat{u}$  is smooth, it is known that  $\hat{u}$  can be approximated well by a shallow NN, i.e., with depth L=2 (see, e.g., [13, 20, 21, 23, 12, 15]).

Remark 4.6. The estimate in (4.7) holds even for the shallow neural network (L=2). However, the second term of the upper bound,  $\inf_{v \in \mathcal{M}(d,1,2,n)} \|\hat{u} + p - v\|_{\beta}$ , depends on the inverse of  $\varepsilon$  because the p has a sharp transition layer of width  $\varepsilon$ . For any fixed n,  $\inf_{v \in \mathcal{M}(d,1,2,n)} \|p - v\|_{0,\Omega}$  could be large depending on the size of  $\varepsilon$ , even though the universal approximation theorem (see, e.g., [21]) implies

$$\lim_{n \to \infty} \inf_{v \in \mathcal{M}(d,1,2,n)} ||p - v||_{0,\Omega} = 0.$$

In other words, as  $\varepsilon$  approaches 0, p approaches  $\chi$ , which is discontinuous; hence, in practice, the universal approximation theorem does not guarantee the convergence of the problem. On the other hand, by Proposition 2.1, deeper networks (with depth at least  $\lceil \log_2(d+1) \rceil + 1$ ) are capable of approximating the solution. As an illustration, define a CPWL function p(x,y) with a sharp transition layer of width  $\varepsilon$  in  $[0,1]^2$  as follows.

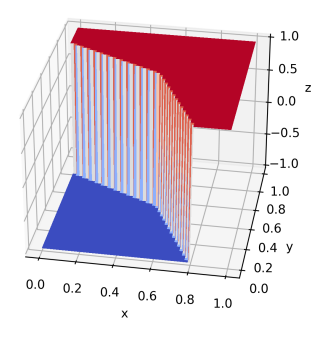
$$p(x,y) = \begin{cases} -1 + \frac{2}{\varepsilon} \left( y + \frac{1}{2}x - 0.8 + \frac{\varepsilon}{2} \right), & y \ge x, \\ -1 + \frac{2}{\varepsilon} \left( \frac{1}{2}y + x - 0.8 + \frac{\varepsilon}{2} \right), & y < x. \end{cases}$$

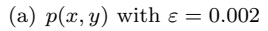
In [7], we proved CPWL functions of the form p(x,y) can be represented by a ReLU DNN with the 2-4-4-1 structure. Here and in what follows, by a 2- $n_1$ - $n_2$ -1 structure, we mean a ReLU DNN with depth 3 and  $n_1$ ,  $n_2$  neurons in the respective hidden layers. Therefore, we can expect the 2- $n_1$ - $n_2$ -1 structure outperforms the 2- $n_3$ -1 structure (ReLU DNNs with depth 2 and  $n_3$  neurons in the hidden layer), and Figure 3 and Table 1 demonstrate this for approximating p(x,y) with  $\varepsilon = 0.2, 0.02, 0.002$  by ReLU DNNs with depth 2, 3 and various numbers of nuerons.

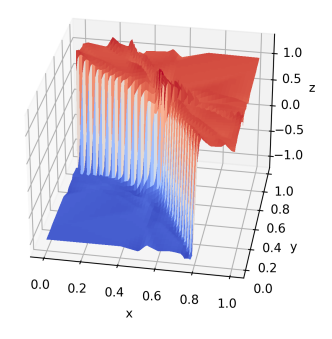
Table 1

Relative errors in the  $L^2$  norm for ReLU DNNs with depth 2, 3 and various numbers of neurons approximating p(x,y) with  $\varepsilon=0.2,0.02,0.002$ 

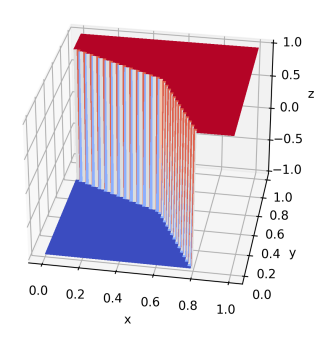
	2-8-1	2-58-1	2-108-1	2-158-1	2-4-4-1
$\varepsilon = 0.2$	0.292446	0.028176	0.021200	0.010259	$1.906427 \times 10^{-7}$
$\varepsilon = 0.02$	0.254603	0.078549	0.065465	0.030623	$7.536140 \times 10^{-6}$
$\varepsilon = 0.002$	0.404299	0.102757	0.100136	0.088885	$9.473783 \times 10^{-7}$



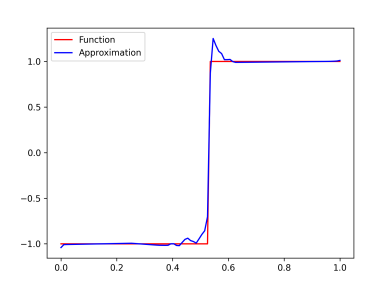




(b) ReLU DNN with the 2-158-1 structure



(c) ReLU DNN with the 2-4-4-1 structure



(d) Trace of 3(b) on y = x

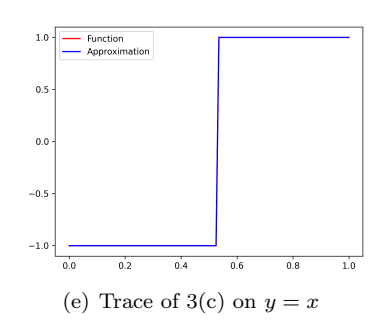


Fig. 3.  $L^2$  norm approximation results of p(x,y) with  $\varepsilon = 0.002$ 

Lemma 4.7. Let u, u<sub>N</sub>, and u<sup>N</sup><sub> $\tau$ </sub> be the solutions of problems (3.2), (3.6), and (3.8), respectively. Then there exist positive constants  $C_1$  and  $C_2$  such that

$$\|u - u_{\tau}^{N}\|_{\beta} \leq C_{1} \left(\left|(\mathcal{L} - \mathcal{L}_{\tau})(u_{N} - u_{\tau}^{N}, \mathbf{0})\right| + \left|(\mathcal{L} - \mathcal{L}_{\tau})(u - u_{N}, \mathbf{0})\right|\right)^{1/2}$$

$$+ C_{2} \left(\left|\alpha_{1} - \alpha_{2}\right| \sqrt{\varepsilon} + \inf_{v \in \mathcal{M}(d, n)} \|\hat{u} + p - v\|_{\beta}\right).$$

$$(4.9)$$

*Proof.* By the triangle inequality

$$\left|\left|\left|u-u_{\tau}^{\scriptscriptstyle N}\right|\right|\right|_{\pmb{\beta}}\leq\left|\left|\left|u-u_{\scriptscriptstyle N}\right|\right|\right|_{\pmb{\beta}}+\left|\left|\left|u_{\scriptscriptstyle N}-u_{\tau}^{\scriptscriptstyle N}\right|\right|\right|_{\pmb{\beta}},$$

and the fact that

$$\left\|\left|\left|u_{\scriptscriptstyle N}-u_{\scriptscriptstyle T}^{\scriptscriptstyle N}\right|\right|_{\boldsymbol{\beta}} \leq C_1 \left(\left(\left|\left(\mathcal{L}-\mathcal{L}_{\scriptscriptstyle T}\right)(u_{\scriptscriptstyle N}-u_{\scriptscriptstyle T}^{\scriptscriptstyle N},\mathbf{0})\right|+\left|\left(\mathcal{L}-\mathcal{L}_{\scriptscriptstyle T}\right)(u-u_{\scriptscriptstyle N},\mathbf{0})\right|\right)^{1/2}+\left\|\left|u-u_{\scriptscriptstyle N}\right|\right\|_{\boldsymbol{\beta}}\right)$$

from the proof of Lemma 3.4 in [7], (4.9) is a direct consequence of Theorem 4.4.

5. Numerical Experiments. In this section, we report the numerical results for both two and three dimensional test problems with piecewise constant, or variable advection velocity fields. Numerical integration uses the midpoint rule on a uniform mesh with mesh size  $h = 10^{-2}$ . The directional derivative  $v_{\beta}$  in the  $\beta$  direction is approximated by the backward finite difference quotient multiplied by  $|\beta|$ 

(5.1) 
$$v_{\beta}(\mathbf{x}_{K}) \approx |\beta| \frac{v(\mathbf{x}_{K}) - v(\mathbf{x}_{K} - \rho \overline{\beta}(\mathbf{x}_{K}))}{\rho},$$

where  $\bar{\beta} = \frac{\beta}{|\beta|}$  and  $\rho = h/4$ . We use the ADAM optimization algorithm [17] to iteratively solve the discrete minimization problem in (3.8). For each numerical experiment, the learning rate starts with 0.004 and is reduced by half for every 50000 iterations. Due to the possibility of the neural network getting trapped in a local minimum, we first train the network with 5000 iterations 10 times, choose the weights and biases with the minimum loss function value, and train further to get the results.

In Tables Tables 2 to 7, parameters indicate the total number of weights and biases. We use ReLU DNN with width n and depth  $3 = \lceil \log_2(d+1) \rceil + 1$  for d=2,3, the structure of DNNs is denoted by d-n-n-1, where the 1 is the dimension of the output. The basic principle for choosing the number of neurons is to start with a small number and increase the number to obtain a better approximation. For an automatic approach to design the architecture of DNNs for a given problem with a prescribed accuracy, see the recent work on the adaptive neural network method in [18, 8]. In Figures 4 to 9, by the  $l^{\text{th}}$  layer breaking lines, we mean the set

$$\{\mathbf{x} \in \Omega : \boldsymbol{\omega}^{(l)}(N^{(l-1)} \circ \cdots \circ N^{(2)} \circ N^{(1)}(\mathbf{x})) - \mathbf{b}^{(l)} = 0\}.$$

**5.1. Two Dimensional Problems.** We present the numerical results for four two dimensional test problems with piecewise constant or variable advection velocity fields. All four test problems are defined on the domain  $\Omega = (0,1)^2$  with  $\gamma = 1$ , and the exact solutions are the same as the right-hand side functions, u(x,y) = f(x,y), which are the step functions (except for the fourth test problem) along three-line segment, four-line segment, and curve interfaces. By Theorem 4.4, the LSNN method with three-layer DNN leads to

$$\| u - u_N \|_{\beta} \le C |\alpha_1 - \alpha_2| \sqrt{\varepsilon},$$

because the continuous part of the solution  $\hat{u}$  is zero (except for the fourth test problem).

**5.1.1. Problem with a three-line segment interface.** This example is a modification of one from [7]. Let  $\bar{\Omega} = \bar{\Upsilon}_1 \cup \bar{\Upsilon}_2 \cup \bar{\Upsilon}_3$  and

$$\Upsilon_1 = \{(x,y) \in \Omega : y \geq x\}, \ \Upsilon_2 = \{(x,y) \in \Omega : x - \frac{a}{2} \leq y < x\}, \ \text{and} \ \Upsilon_3 = \{(x,y) \in \Omega : y < x - \frac{a}{2}\}$$

with a = 43/64. The advective velocity field is a piecewise constant field given by

(5.2) 
$$\boldsymbol{\beta}(x,y) = \left\{ \begin{array}{ll} (-1,\sqrt{2}-1)^T, & (x,y) \in \Upsilon_1, \\ (1-\sqrt{2},1)^T, & (x,y) \in \Upsilon_2, \\ (-1,\sqrt{2}-1)^T, & (x,y) \in \Upsilon_3. \end{array} \right.$$

The inflow boundary and the inflow boundary condition are given by

$$\Gamma_{-} = \{(1, y) : y \in (0, 1)\} \cup \{(x, 0) : x \in (0, 1)\}$$
and 
$$g(x, y) = \begin{cases} 1, & (x, y) \in \Gamma_{-}^{1} \equiv \{(1, y) : y \in [1 - \sqrt{2} + \frac{\sqrt{2}}{2}a, 1)\}, \\ -1, & (x, y) \in \Gamma_{-}^{2} = \Gamma_{-} \setminus \Gamma_{-}^{1}, \end{cases}$$

respectively. Let

$$\hat{\Upsilon}_1 = \{(x,y) \in \Upsilon_1 : y < (1-\sqrt{2})x + a\}, \ \hat{\Upsilon}_2 = \{(x,y) \in \Upsilon_2 : y < \frac{1}{1-\sqrt{2}}(x-\frac{a}{\sqrt{2}}) + \frac{a}{\sqrt{2}}\},$$

and 
$$\hat{\Upsilon}_3 = \{(x,y) \in \Upsilon_3 : y < (1 - \sqrt{2})x + \frac{\sqrt{2}}{2}a\}.$$

The following right-hand side function is

(5.3) 
$$f(x,y) = \begin{cases} -1, & (x,y) \in \Omega_1 \equiv \hat{\Upsilon}_1 \cup \hat{\Upsilon}_2 \cup \hat{\Upsilon}_3, \\ 1, & (x,y) \in \Omega_2 = \Omega \setminus \Omega_1. \end{cases}$$

The LSNN method with a random initialization and 200000 iterations is implemented with 2-300-1 and 2-5-5-1 networks. The numerical results are presented in Figure 4 and Table 2. The numerical error (Table 2), trace (Figure 4(e)), and approximation graph (Figure 4(c)) of the 2-layer network imply that the 2-layer network structure fails to approximate the solution especially around the discontinuous interface (Figure 4(a)), although the breaking lines (Figure 4(g)) indicate the network tried to find the discontinuous interface. This and the remaining examples suggest the 2-layer network structure may not be able to approximate discontinuous solutions well as we expected in Remark 4.6. On the other hand, the 3-layer network with the 2-5-5-1 structure with 4% of parameters of the 2-layer network approximates the solution accurately. Again, this and the remaining examples suggest that 3-layer networks may be more efficient than 2-layer ones of even bigger sizes. In this example, because of the structure of the interface and  $\hat{u}=0$ , the function p with small  $\varepsilon$  that we constructed in Lemma 4.3 is a good approximation of the solution, and Figure 4(d) indicates that the approximation is indeed such a function and is contained in  $\mathcal{M}(2,1,3,10)$ . The trace (Figure 4(f)) of the 3-layer network exhibits no oscillation and the second layer breaking lines (Figure 4(h)) show the location of the interface.

Table 2
Relative errors of the problem with a 3-line segment interface

Network structure	$\frac{\ u\!-\!u_{\mathcal{T}}^N\ _0}{\ u\ _0}$	$\frac{\left\ \left\ u-u_{\mathcal{T}}^{N}\right\ \right\ _{\boldsymbol{\beta}}}{\left\ \left\ u\right\ \right\ _{\boldsymbol{\beta}}}$	$\frac{\mathcal{L}^{1/2}(u_{\mathcal{T}}^{N},\mathbf{f})}{\mathcal{L}^{1/2}(u_{\mathcal{T}}^{N},0)}$	Parameters
2-300-1	0.279867	0.404376	0.300774	1201
2-5-5-1	0.074153	0.079193	0.044987	51

# **5.1.2.** Problem with a 4 line segment interface. Let $\bar{\Omega} = \bar{\Upsilon}_1 \cup \bar{\Upsilon}_2 \cup \bar{\Upsilon}_3 \cup \bar{\Upsilon}_4$ and

$$\Upsilon_1 = \{(x, y) \in \Omega : y \ge x + 1\}, \ \Upsilon_2 = \{(x, y) \in \Omega, \ x \le y < x + 1\},$$

$$\Upsilon_3 = \{(x, y) \in \Omega, \ x - 1 \le y < x\}, \ \text{and} \ \Upsilon_4 = \{(x, y) \in \Omega, \ y < x - 1\}.$$

The advective velocity field is a piecewise constant field given by

(5.4) 
$$\boldsymbol{\beta}(x,y) = \begin{cases} (-1,\sqrt{2}-1)^T, & (x,y) \in \Upsilon_1, \\ (1-\sqrt{2},1)^T, & (x,y) \in \Upsilon_2, \\ (-1,\sqrt{2}-1)^T, & (x,y) \in \Upsilon_3, \\ (1-\sqrt{2},1)^T, & (x,y) \in \Upsilon_4. \end{cases}$$

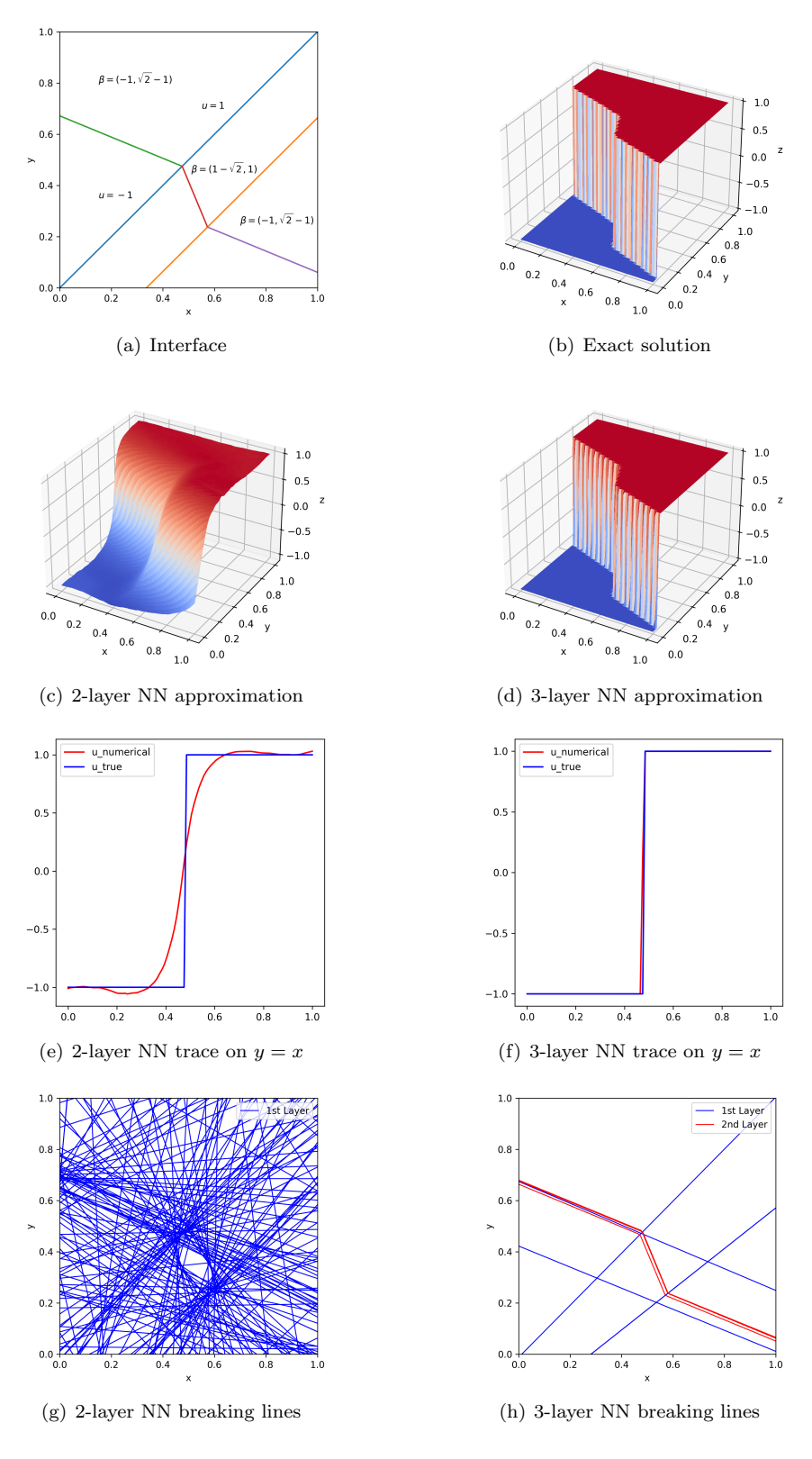


Fig. 4. Approximation results of the problem with a 3-line segment interface

The inflow boundary and the inflow boundary condition are given by

$$\Gamma_{-} = \{(2, y) : y \in (0, 2)\} \cup \{(x, 0) : x \in (0, 2)\}$$
and 
$$g(x, y) = \begin{cases} 1, & (x, y) \in \Gamma_{-}^{1} \equiv \{(2, y) : y \in (0, 2)\}, \\ -1, & (x, y) \in \Gamma_{-}^{2} = \Gamma_{-} \setminus \Gamma_{-}^{1}, \end{cases}$$

respectively. Let

$$\hat{\Upsilon}_1 = \{(x,y) \in \Upsilon_1 : y < (1-\sqrt{2})x+2\}, \ \hat{\Upsilon}_2 = \{(x,y) \in \Upsilon_2 : y < \frac{1}{1-\sqrt{2}}(x-1)+1\},$$

$$\hat{\Upsilon}_3 = \{(x,y) \in \Upsilon_3 : y < (1-\sqrt{2})(x-1)+1\}, \text{ and } \hat{\Upsilon}_4 = \{(x,y) \in \Upsilon_3 : y < \frac{1}{1-\sqrt{2}}x+\frac{2}{\sqrt{2}-1}\}.$$

The following right-hand side function is

(5.5) 
$$f(x,y) = \begin{cases} -1, & (x,y) \in \Omega_1 \equiv \hat{\Upsilon}_1 \cup \hat{\Upsilon}_2 \cup \hat{\Upsilon}_3 \cup \hat{\Upsilon}_4, \\ 1, & (x,y) \in \Omega_2 = \Omega \setminus \Omega_1. \end{cases}$$

The LSNN method with a random initialization and 200000 iterations is implemented with 2-300-1 and 2-6-6-1 networks. The numerical results are presented in Figure 5 and Table 3. Since the interface has one more line segment than Example 5.1.1, we increase the number of neurons to have higher expresiveness. The 2-6-6-1 network with 6% of parameters of the 2-300-1 network approximates the solution accurately and Figure 5(d) indicates the approximation is the function p with small  $\varepsilon$  and contained in  $\mathcal{M}(2,1,3,12)$ . The trace (Figure 5(f)) shows no oscillation and the second layer breaking lines (Figure 5(h)) are consistent with the interface (Figure 5(a)). On the other hand, the 2-300-1 network again roughly finds the location of the interface (Figure 5(g)) but does not approximate the solution well (Figures 5(c) and 5(e) and Table 3).

Table 3
Relative errors of the problem with a 4-line segment interface

Network structure	$\frac{\ u - u_{\mathcal{T}}^N\ _0}{\ u\ _0}$	$\frac{\left\ \left\ u-u_{\mathcal{T}}^{N}\right\ \right\ _{\boldsymbol{\beta}}}{\left\ \left\ u\right\ \right\ _{\boldsymbol{\beta}}}$	$\frac{\mathcal{L}^{1/2}(u_{\mathcal{T}}^{N},\mathbf{f})}{\mathcal{L}^{1/2}(u_{\mathcal{T}}^{N},0)}$	Parameters
2-300-1	0.288282	0.358756	0.306695	1201
2-6-6-1	0.085817	0.091800	0.069808	67

**5.1.3. Problem with a curve interface.** The advective velocity field is a variable field given by

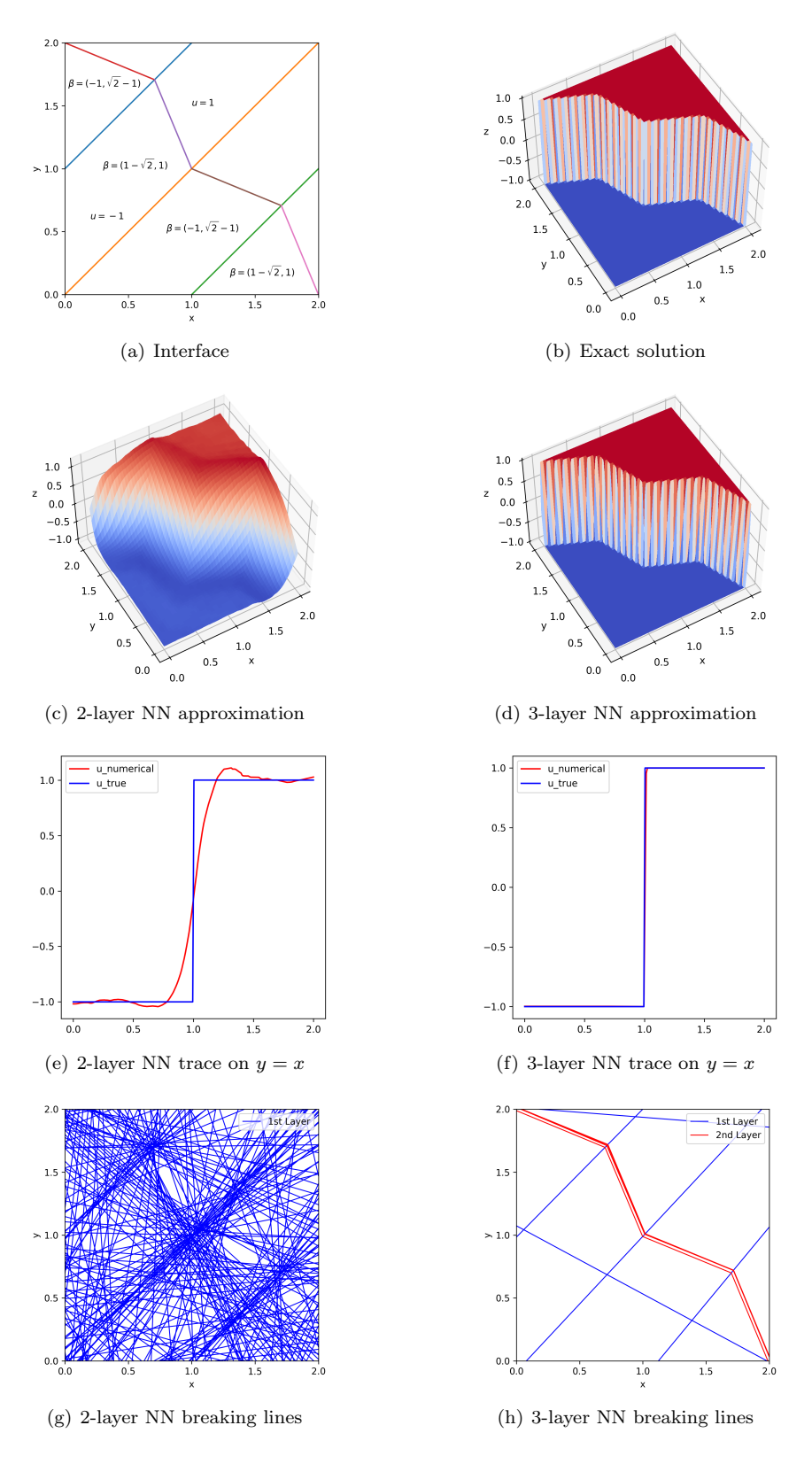
(5.6) 
$$\beta(x,y) = (1,2x), (x,y) \in \Omega.$$

The inflow boundary and the inflow boundary condition are given by

$$\Gamma_{-} = \{(0, y) : y \in (0, 1)\} \cup \{(x, 0) : x \in (0, 1)\}$$
and 
$$g(x, y) = \begin{cases} 1, & (x, y) \in \Gamma_{-}^{1} \equiv \{(0, y) : y \in [\frac{1}{8}, 1)\}, \\ 0, & (x, y) \in \Gamma_{-}^{2} = \Gamma_{-} \setminus \Gamma_{-}^{1}, \end{cases}$$

respectively. The following right-hand side function is

(5.7) 
$$f(x,y) = \begin{cases} 0, & (x,y) \in \Omega_1 \equiv \{(x,y) \in \Omega : y < x^2 + \frac{1}{8}\}, \\ 1, & (x,y) \in \Omega_2 = \Omega \setminus \Omega_1. \end{cases}$$



 $Fig.\ 5.\ Approximation\ results\ of\ the\ problem\ with\ a\ 4-line\ segment\ interface$ 

The LSNN method with a random initialization and 300000 iterations is implemented with 2-3000-1 and 2-60-60-1 networks. We increase the number of neurons for the 3-layer network structure assuming continuous piecewise linear functions approximating a curved discontinuous interface well would be a ReLU DNN with more neurons. The numerical results are presented in Figure 6 and Table 4. Figures 6(c) and 6(e) suggest the 2-layer network structure fails to approximate the solution around the discontinuous interface even with three times more parameters than the 3-layer network structure. In contrast, the 3-layer network structure shows better numerical errors (Table 4), pointwise approximations (Figures 6(d) and 6(f)) locating the discontinuous interface well (Figure 6(h)).

 ${\it TABLE~4} \\ Relative~errors~of~the~problem~with~a~curve~interface$ 

Network structure	$\frac{\ u - u_{\mathcal{T}}^N\ _0}{\ u\ _0}$	$\frac{\left\ \left\ u-u_{\mathcal{T}}^{N}\right\ \right\ _{\boldsymbol{\beta}}}{\left\ \left\ u\right\ \right\ _{\boldsymbol{\beta}}}$	$\frac{\mathcal{L}^{1/2}(u_{\mathcal{T}}^{N},\mathbf{f})}{\mathcal{L}^{1/2}(u_{\mathcal{T}}^{N},0)}$	Parameters
2-3000-1	0.134514	0.181499	0.078832	12001
2-60-60-1	0.066055	0.106095	0.030990	3901

**5.1.4. Problem with a curve interface where**  $\hat{u} \neq 0$ **.** The advective velocity field is a variable field given by

$$\beta(x,y) = (-y,x), (x,y) \in \Omega.$$

The inflow boundary and the inflow boundary condition are given by

$$\Gamma_{-} = \{(1, y) : y \in (0, 1)\} \cup \{(x, 0) : x \in (0, 1)\}$$
and 
$$g(x, y) = \begin{cases} -1 + x^2 + y^2, & (x, y) \in \Gamma_{-}^1 \equiv \{(x, 0) : x \in (0, \frac{2}{3})\}, \\ 1 + x^2 + y^2, & (x, y) \in \Gamma_{-}^2 = \Gamma_{-} \setminus \Gamma_{-}^1, \end{cases}$$

respectively. The following right-hand side function is

(5.9) 
$$f(x,y) = \begin{cases} -1 + x^2 + y^2, & (x,y) \in \Omega_1 \equiv \{(x,y) \in \Omega : y < \sqrt{\frac{4}{9} - x^2}\}, \\ 1 + x^2 + y^2, & (x,y) \in \Omega_2 = \Omega \setminus \Omega_1. \end{cases}$$

The LSNN method with a random initialization and 200000 iterations is implemented with 2-4000-1 and 2-65-65-1 networks. The numerical results are presented in Figure 7 and Table 5. Table 5 indicates the 2-layer network is capable of approximating the solution in average but Figures 7(c) and 7(e) show difficulty around the discontinuous interface. Again, the 3-layer network with 28% of parameters of the 2-layer network presents better errors (Table 5) and approximates the solution accurately pointwise (Figures 7(d) and 7(f)). Unlike other examples, some of the second layer breaking lines of the network (Figure 7(h)) are spread out in the whole domain in addition to those around the interface, which implies they are necessary for approximating the solution with  $\hat{u} \neq 0$ .

5.2. Three Dimensional Problems. We present the numerical results for two three dimensional test problems with piecewise constant or variable advection velocity fields whose solutions are piecewise constant along a connected series of planes or a surface. All three test problems are defined on the domain  $\Omega = (0, 1)^3$ , and again, we have

$$\| u - u_{N} \|_{\beta} \le C |\alpha_{1} - \alpha_{2}| \sqrt{\varepsilon}.$$

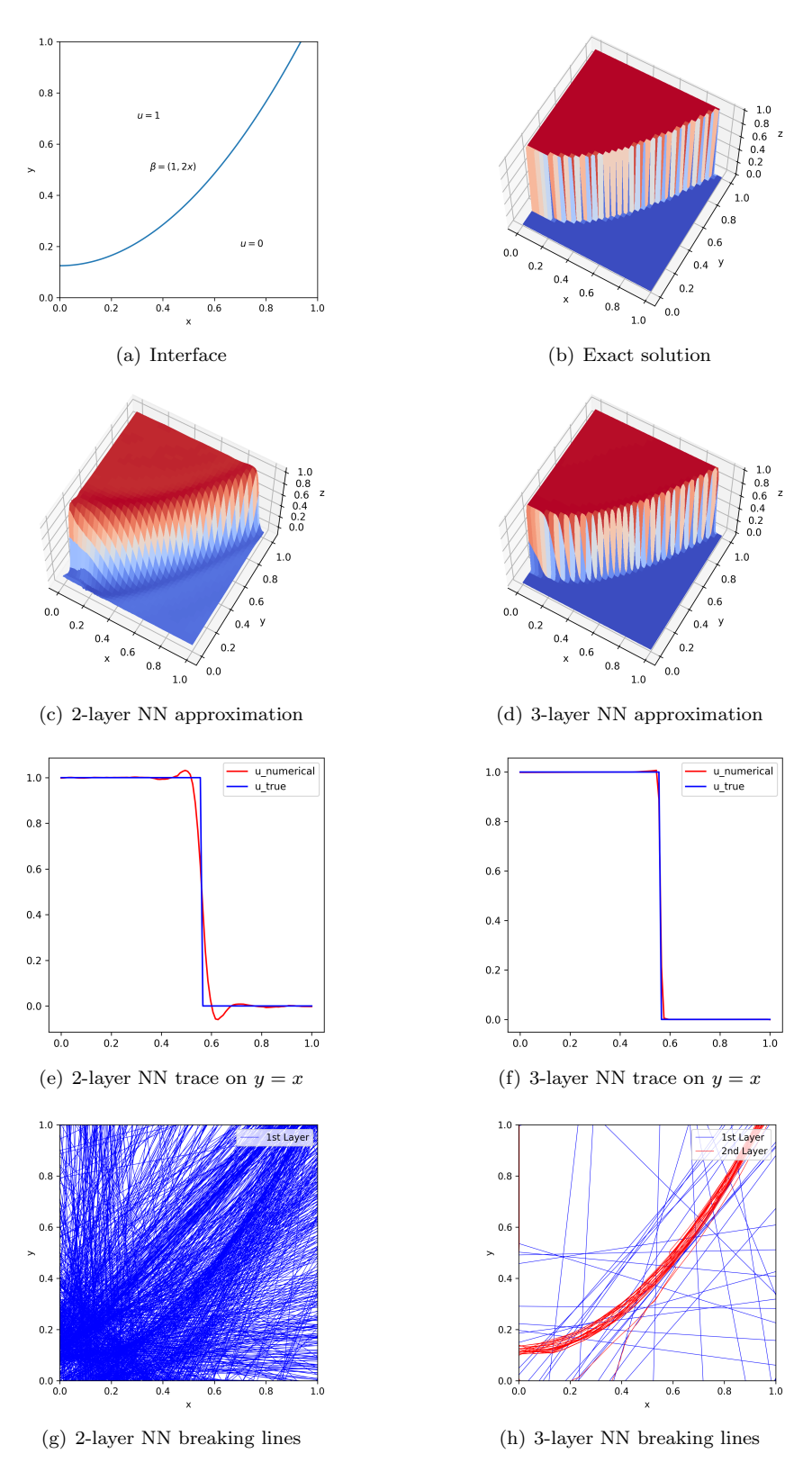


Fig. 6. Approximation results of the problem with a curve interface

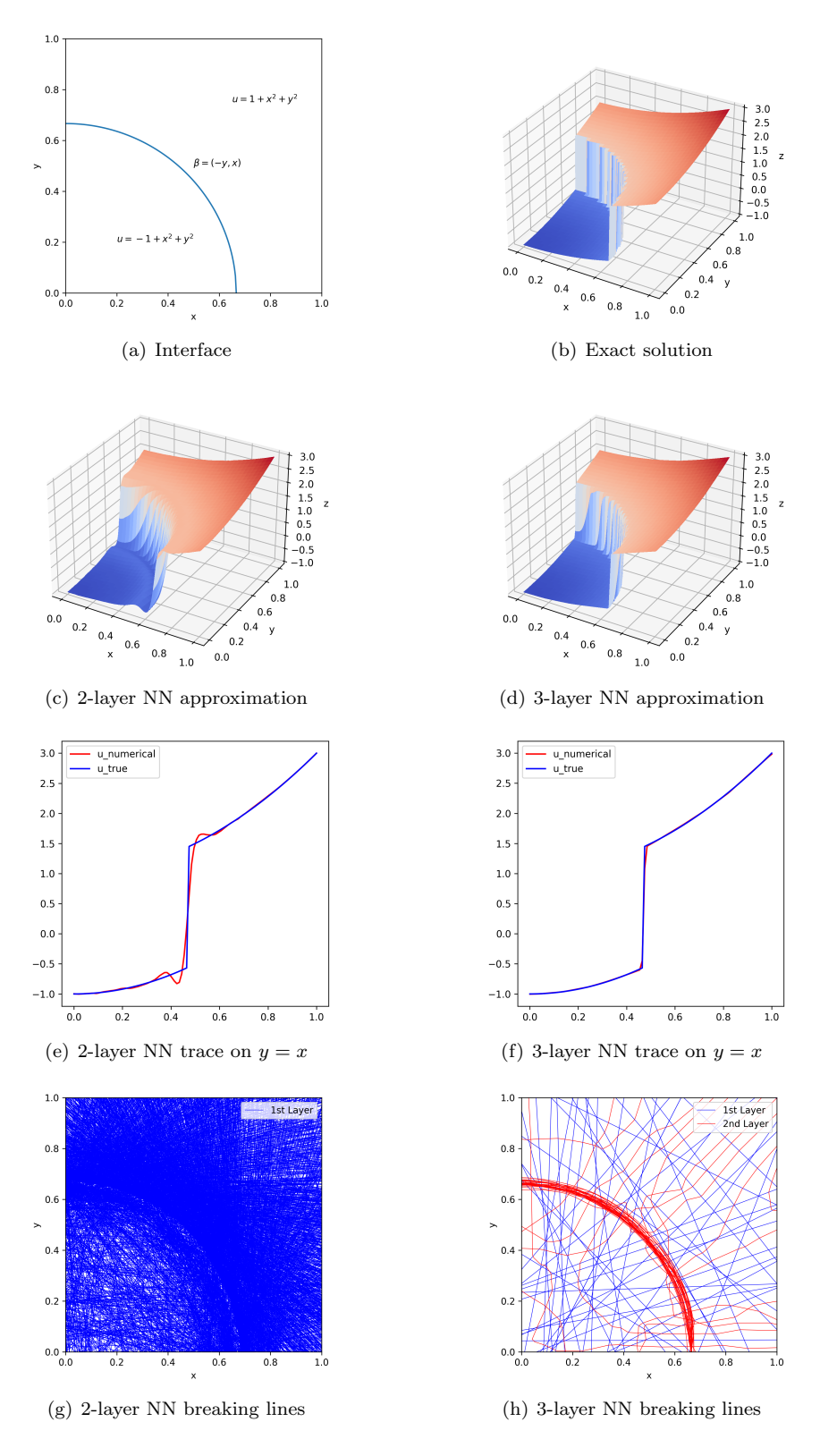


Fig. 7. Approximation results of the problem with a curve interface where  $\hat{u} \neq 0$ 

Network structure	$\frac{\ u\!-\!u_{\mathcal{T}}^N\ _0}{\ u\ _0}$	$\frac{\left\ \left\ u-u_{\mathcal{T}}^{N}\right\ \right\ _{\boldsymbol{\beta}}}{\left\ \left\ u\right\ \right\ _{\boldsymbol{\beta}}}$	$\frac{\mathcal{L}^{1/2}(u_{\mathcal{T}}^N,\mathbf{f})}{\mathcal{L}^{1/2}(u_{\mathcal{T}}^N,0)}$	Parameters
2-4000-1	0.088349	0.108430	0.058213	16001
2-65-65-1	0.048278	0.073095	0.015012	4551

### **5.2.1. Problem with a piecewise plane interface.** Let $\gamma = f = 0$ , $\bar{\Omega} = \bar{\Upsilon}_1 \cup \bar{\Upsilon}_2$ , and

$$\Upsilon_1 = \{(x, y, z) \in \Omega : y < x\}, \ \Upsilon_2 = \{(x, y, z) \in \Omega : y \ge x\}.$$

The advective velocity field is a piecewise constant field given by

(5.10) 
$$\boldsymbol{\beta}(x, y, z) = \begin{cases} (1 - \sqrt{2}, 1, 0)^T, & (x, y, z) \in \Upsilon_1 \\ (-1, \sqrt{2} - 1, 0)^T, & (x, y, z) \in \Upsilon_2. \end{cases}$$

The inflow boundary and the inflow boundary condition are given by

$$\Gamma_{-} = \{(x, 0, z) : x, z \in (0, 1)\} \cup \{(1, y, z) : y, z \in (0, 1)\}$$
and 
$$g(x, y, z) = \begin{cases} 0, & (x, y, z) \in \Gamma_{-}^{1} \equiv \{(x, 0, z) : x \in (0, 0.7), z \in (0, 1)\}, \\ 1, & (x, y, z) \in \Gamma_{-}^{2} = \Gamma_{-} \setminus \Gamma_{-}^{1}, \end{cases}$$

respectively. Let

$$\Omega_1 = \{(x, y, z) \in \Omega : y < (1 - \sqrt{2})x + 0.7, \ y < \frac{1}{1 - \sqrt{2}}(x - 0.7)\}.$$

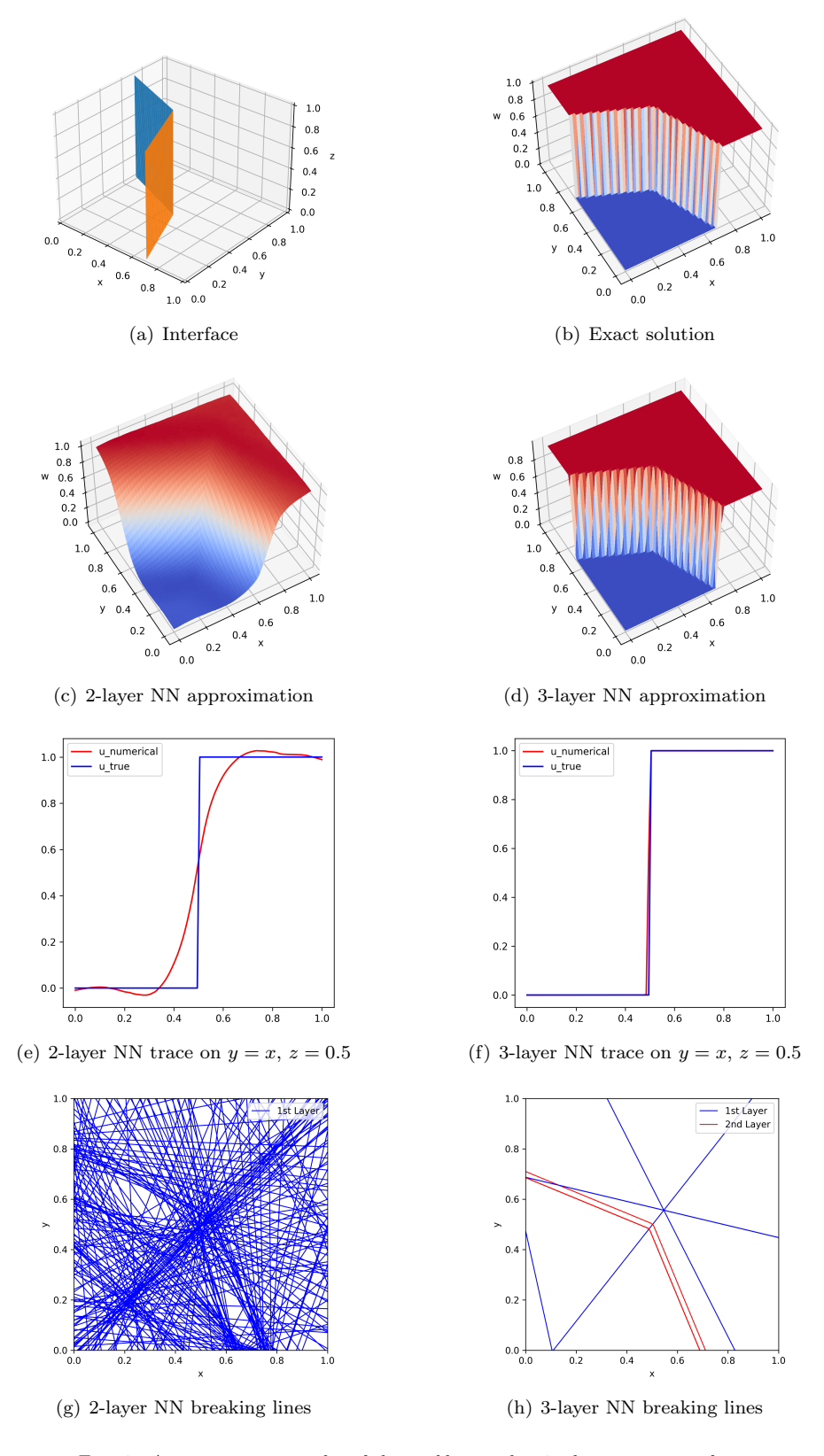
The exact solution is a unit step function in three dimensions

(5.11) 
$$u(x, y, z) = \begin{cases} 0, & (x, y, z) \in \Omega_1, \\ 1, & (x, y, z) \in \Omega_2 = \Omega \setminus \Omega_1. \end{cases}$$

The LSNN method with a random initialization and 100000 iterations is implemented with 3-300-1 and 3-5-5-1 networks (depth  $3 = \lceil \log_2(d+1) \rceil + 1$  for d=3). Again for three dimensions, the 2-layer structure with a large number of parameters knows the location of discontinuous interface (Figures 8(a) and 8(g)) but shows difficulty approximating the solution accurately around the interface (Figures 8(c) and 8(e)). The 3-layer network structure with 4% of parameters of the 2-layer network approximates the solution accurately without oscillation (Table 6). As explained in Example 5.1.1, Figures 8(d), 8(f), and 8(h) also indicate the function p seems to be an approximation and in this example, contained in  $\mathcal{M}(3,1,3,10)$ .

Table 6
Relative errors of the problem with a 2-plane piece interface

Network structure	$\frac{\ u\!-\!u_{\mathcal{T}}^N\ _0}{\ u\ _0}$	$\frac{\left\ \left\ u-u_{\mathcal{T}}^{N}\right\ \right\ _{\boldsymbol{\beta}}}{\left\ \left\ u\right\ \right\ _{\boldsymbol{\beta}}}$	$rac{\mathcal{L}^{1/2}(u_{\mathcal{T}}^N,\mathbf{f})}{\mathcal{L}^{1/2}(u_{\mathcal{T}}^N,0)}$	Parameters
3-300-1	0.185006	0.214390	0.189820	1501
3-5-5-1	0.055365	0.055370	0.045902	56



 $Fig.\ 8.\ Approximation\ results\ of\ the\ problem\ with\ a\ 2-plane\ piece\ interface$ 

**5.2.2. Problem with a cylindrical interface.** Let  $\gamma = 1$ . The advective velocity field is a variable field given by

(5.12) 
$$\beta(x, y, z) = (-y, x, 0)^T, (x, y, z) \in \Omega.$$

The inflow boundary and the inflow boundary condition are given by

$$\Gamma_{-} = \{(x,0,z) : x,z \in (0,1)\} \cup \{(1,y,z) : y,z \in (0,1)\}$$
 and 
$$g(x,y,z) = \begin{cases} 0, & (x,y,z) \in \Gamma_{-}^{1} \equiv \{(x,0,z) : x \in (0,0.7), z \in (0,1)\}, \\ 1, & (x,y,z) \in \Gamma_{-}^{2} = \Gamma_{-} \setminus \Gamma_{-}^{1}. \end{cases}$$

respectively. Let

$$\Omega_1 = \{(x, y, z) \in \Omega : y < \sqrt{0.7^2 - x^2}.\}$$

The following right-hand side function is

(5.13) 
$$f(x,y,z) = \begin{cases} 0, & (x,y,z) \in \Omega_1, \\ 1, & (x,y,z) \in \Omega_2 = \Omega \setminus \Omega_1. \end{cases}$$

The exact solution is

$$u(x, y, z) = f(x, y, z), (x, y, z) \in \Omega.$$

The LSNN method with a random initialization and 150000 iterations is implemented with 3-1500-1 and 3-50-50-1 networks. Again to minimize the loss function over a larger subset of CPWL functions, we increase the number of neurons. The numerical results are presented in Figure 9 and Table 7. Even though the 2-layer network indicates an approximate location of the discontinuous interface (Figures 9(a) and 9(g)), it fails to approximate the solution around the interface. The 3-layer network with less than 40% of parameters approximates the solution well locating the discontinuous interface (Figures 9(d), 9(f), and 9(h) and Table 7).

Table 7
Relative errors of the problem with a cylindrical interface

Network structure	$\frac{\ u - u_{\mathcal{T}}^N\ _0}{\ u\ _0}$	$\frac{\left\ \left\ u-u_{\mathcal{T}}^{N}\right\ \right\ _{\boldsymbol{\beta}}}{\left\ \left\ u\right\ \right\ _{\boldsymbol{\beta}}}$	$\frac{\mathcal{L}^{1/2}(u_{\mathcal{T}}^{N},\mathbf{f})}{\mathcal{L}^{1/2}(u_{\mathcal{T}}^{N},0)}$	Parameters
3-1500-1	0.125142	0.158393	0.117929	7501
3-50-50-1	0.050217	0.073780	0.018976	2801

#### 6. Conclusions.

#### REFERENCES

- R. Arora, A. Basu, P. Mianjy, and A. Mukherjee, Understanding deep neural networks with rectified linear units, arXiv preprint arXiv:1611.01491, (2016), https://doi.org/10.48550/arXiv.1611.01491.
- Y. BAR-SINAI, S. HOYER, J. HICKEY, AND M. P. BRENNER, Learning data-driven discretizations for partial differential equations, Proc. Natl. Acad. Sci. USA, 116 (31) (2019), pp. 15344–15349, https://doi.org/10. 1073/pnas.1814058116.
- [3] J. BERG AND K. NYSTRÖM, A unified deep artificial neural network approach to partial differential equations in complex geometries, Neurocomputing, 317 (2018), pp. 28-41, https://doi.org/10.1016/j.neucom.2018. 06.056.
- [4] P. Bochev and M. Gunzburger, Least-squares methods for hyperbolic problems, in Handb. Numer. Anal., vol. 17, Elsevier, 2016, pp. 289–317, https://doi.org/10.1016/bs.hna.2016.07.002.
- [5] Z. CAI, J. CHEN, AND M. LIU, Least-squares ReLU neural network (LSNN) method for scalar nonlinear hyperbolic conservation law, Appl. Numer. Math., 174 (2022), pp. 163–176, https://doi.org/10.1016/j. apnum.2022.01.002.

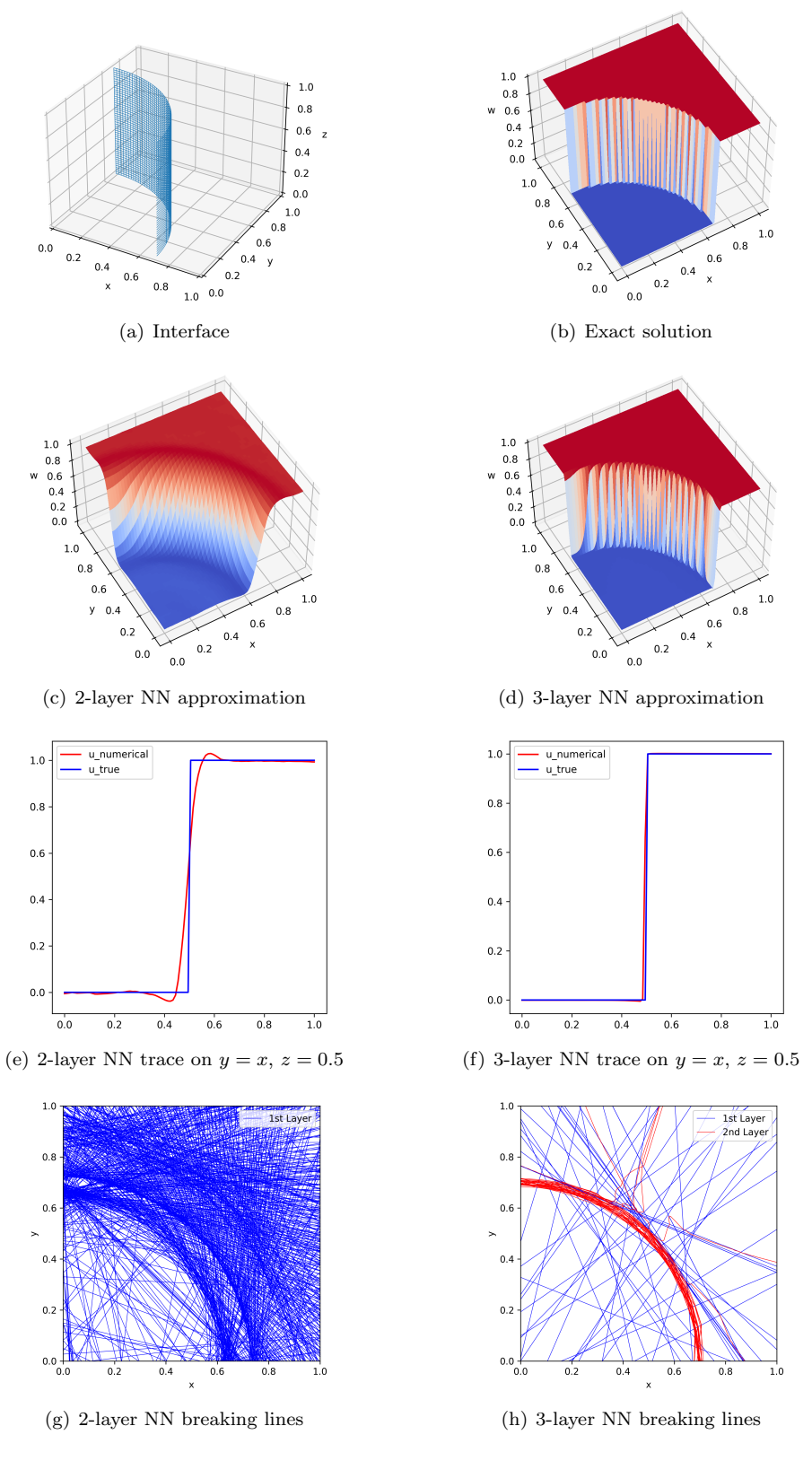


Fig. 9. Approximation results of the problem with a cylindrical interface

- [6] Z. Cai, J. Chen, and M. Liu, LSNN method for scalar nonlinear HCLs: discrete divergence operator, arXiv preprint arXiv:2110.10895v2 [math.NA], (2022), https://doi.org/10.48550/arXiv.2110.10895.
- [7] Z. Cai, J. Chen, and M. Liu, Least-squares ReLU neural network (LSNN) method for linear advectionreaction equation, J. Comput. Phys., (443 (2021) 110514), https://doi.org/10.1016/j.jcp.2021.110514.
- [8] Z. CAI, J. CHEN, AND M. LIU, Self-adaptive deep neural network: Numerical approximation to functions and PDEs, J. Comput. Phys., (455 (2022) 111021), https://doi.org/10.1016/j.jcp.2022.111021.
- Z. CAI, J. CHEN, M. LIU, AND X. LIU, Deep least-squares methods: An unsupervised learning-based numerical method for solving elliptic PDEs, J. Comput. Phys., 420 (2020), p. 109707, https://doi.org/10.1016/j.jcp. 2020.109707.
- [10] W. DAHMEN, C. HUANG, C. SCHWAB, AND G. WELPER, Adaptive petrov-galerkin methods for first order transport equations, SIAM J. Numer. Anal., 50 (2012), pp. 2420–2445, https://doi.org/10.1137/110823158.
- [11] H. DE STERCK, T. A. MANTEUFFEL, S. F. MCCORMICK, AND L. OLSON, Least-squares finite element methods and algebraic multigrid solvers for linear hyperbolic PDEs, SIAM J. Sci. Comput., 26 (2004), pp. 31–54, https://doi.org/10.1137/S106482750240858X.
- [12] R. DEVORE, B. HANIN, AND G. PETROVA, Neural network approximation, Acta Numer., 30 (2021), pp. 327–444, https://doi.org/10.1017/S0962492921000052.
- [13] R. A. DEVORE, K. I. OSKOLKOV, AND P. P. PETRUSHEV, Approximation by feed-forward neural networks, Annals of Numerical Mathematics, 4 (1996), pp. 261–288.
- [14] W. E AND B. Yu, The deep ritz method: A deep learning-based numerical algorithm for solving variational problems, Commun. Math. Stat., 6 (2018), pp. 1–12, https://doi.org/10.1007/s40304-018-0127-z.
- [15] S. Hon and H. Yang, Simultaneous neural network approximations in sobolev spaces, arXiv preprint arXiv:2109.00161v1, (2021), https://doi.org/10.48550/arXiv.2109.00161.
- [16] P. HOUSTON, R. RANNACHER, AND E. SÜLI, A posteriori error analysis for stabilised finite element approximations of transport problems, Comput. Methods Appl. Mech. Engrg., 190 (2000), pp. 1483–1508, https://doi.org/10.1016/S0045-7825(00)00174-2.
- [17] D. P. KINGMA AND J. BA, ADAM: A method for stochastic optimization, in International Conference on Representation Learning, San Diego, 2015.
- [18] M. LIU, Z. CAI, AND J. CHEN, Adaptive two-layer ReLU neural network: I. best least-squares approximation, Comput. Math. Appl., 113 (2022), pp. 34–44, https://doi.org/10.1016/j.camwa.2022.03.005.
- [19] Q. LIU AND S. ZHANG, Adaptive least-squares finite element methods for linear transport equations based on an H(div) flux reformulation, Comput. Methods Appl. Mech. Engrg., (366 (2020) 113041), https://doi.org/10.1016/j.cma.2020.113041.
- [20] P. P. Petrushev, Approximation by ridge functions and neural networks, SIAM J. Math. Anal., 30 (1998), pp. 155–189, https://doi.org/10.1137/S0036141097322959.
- [21] A. PINKUS, Approximation theory of the MLP model in neural networks, Acta Numer., 8 (1999), pp. 143–195, https://doi.org/10.1017/S0962492900002919.
- [22] M. RAISSI, P. PERDIKARIS, AND G. KARNIADAKIS, Physics-informed neural networks: A deep learning framework for solving forward and inverse problems involving nonlinear partial differential equations, J. Comput. Phys., 378 (2019), pp. 686–707, https://doi.org/10.1016/j.jcp.2018.10.045.
- [23] Z. SHEN, H. YANG, AND S. ZHANG, Deep network approximation characterized by number of neurons, arXiv preprint arXiv:1906.05497, (2019), https://doi.org/10.48550/arXiv.1906.05497.
- [24] J. SIRIGNANO AND K. SPILIOPOULOS, DGM: A deep learning algorithm for solving partial differential equations, J. Comput. Phys., 375 (2018), pp. 1139–1364, https://doi.org/10.1016/j.jcp.2018.08.029.
- [25] J. TARELA AND M. MARTINEZ, Region configurations for realizability of lattice piecewise-linear models, Math. Comput. Modelling, 30 (1999), pp. 17–27, https://doi.org/10.1016/S0895-7177(99)00195-8.
- [26] S. WANG AND X. SUN, Generalization of hinging hyperplanes, IEEE Trans. Inform. Theory, 51 (2005), pp. 4425–4431, https://doi.org/10.1109/TIT.2005.859246.